Seismic Analysis of L-shaped Quay Walls Considering Soil-Structure Interaction

A. Gharavi & K. Bargi
School of Civil Engineering, College of Engineering, University of Tehran, Tehran

SUMMARY:
In the current study, the seismic behaviour of L-shaped quay walls is considered in two conditions: with or without counterfort. Numerical modelling in finite elements method (3D solid elements) is used to model the wall and the soil behind it. Wall's elements consist of concrete and reinforcement which have nonlinear behaviour in the seismic analysis. For being more specific in modelling, the reinforcements of the concrete are considered in seismic behaviour of the wall. The soil inelastic behaviour is modelled by using modified Drucker-Prager failure criterion. with different values of friction angle. Moreover, contact surfaces are used for soil-structure interaction in the structural model. The system is subjected to El Centro ground acceleration earthquake record to investigate the effects of soil type and counterfort on seismic response of these structures. The results show that increase in friction angle of soil lead to reduction of the wall deflection. Using retaining walls with counterforts not only can improve the seismic behaviour of the wall but also lead to a more economical design.

Keywords: quay walls, seismic behaviour, soil-structure interaction, finite elements

1. INTRODUCTION

Nowadays it is so important to understand the behaviour of quay walls according to widespread usage of this type of structures in marine environments. The L-shaped retaining wall is a kind of gravity wall which is used with or without counterfort. Moreover the effect of soil-structure interaction could make the modelling more specific and realistic. Use of counterforts for L-shaped walls is very important because it can reduce the thickness of the main cantilever wall on high elevations and make the wall's design more economic.

Behaviour of gravity quay-walls underground excitation was already addressed by a number of researchers. For example Madabhushi and Zeng (1998) numerically studied the seismic response of gravity quay-walls. Dynamic behaviour of caisson type quay-walls was studied by Kuwano et al. (1999) through centrifuge model tests.

Goh (1993) studied the behaviour of cantilever retaining walls and proposed a simplified design procedure for estimating the lateral earth pressures in cantilever retaining walls with loosely placed backfill. Kim et al. (2004) evaluated the magnitude and the phase variation of the dynamic thrust on the back of the wall and verified their results with experimental shaking table test. Kolathayar and Ghosh (2009) investigated the seismic active earth pressure behind the rigid cantilever retaining wall with bilinear backface using pseudo-dynamic approach. Gursoy and Durmus (2009) assessed the linear and nonlinear behaviour of reinforced concrete cantilever retaining walls according to the earthquake loads considering soil-structure interaction.

2. MATERIALS

2.1. Soil modelling

2.1.1. Modified Drucker-Prager cap model

This Model has been introduced by Drucker et al. (1957). Over the years, the DPC plasticity model has been modified and expanded (Chen and Mizuno 1990; Sandler 2002). Fig. 2.1 shows a typical Drucker-Prager cap model (ABAQUS 2006). The model is assumed to be isotropic and its yield surface includes three segments: a shear failure surface, providing dominantly shearing flow. A Cap, providing an inelastic hardening mechanism to represent plastic compaction, and a transition region between these segments, introduced to provide a smooth surface purely for facilitating the numerical implementation.

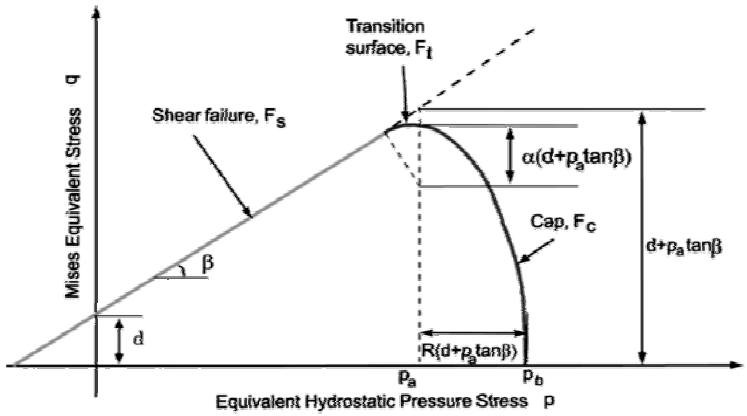

Figure 2.1. Drucker-Prager Cap model: yield surface in the p-q plane (ABAQUS 2006)

2.1.2. Formulas and material parameters

The Drucker-Prager shear failure surface is written as:

$$F_s = q - p.\tan(\beta) - d \tag{2.1}$$

Where β is the material friction angle, d is its cohesion, $p = -\frac{1}{3}\,\mathrm{trace}(\sigma)$ is the hydrostatic pressure stress, and $q = \sqrt{\frac{3}{2}(S:S)}$ is the Mises equivalent stress in which S is the stress deviator, defined as:

$$S = \sigma + pI \tag{2.2}$$

Where σ is the stress tensor, and I is the identity matrix.
For a uniaxial cylindrical die compaction test, the hydrostatic pressure stress and the Mises equivalent stress are expressed as:

$$p = -\frac{1}{3}(\sigma_z + 2\sigma_r) \tag{2.3}$$

$$q = |\sigma_z - \sigma_r| \tag{2.4}$$

Where σ_z and σ_r are the axial and radial stresses, respectively.
The cap serves two main purposes: it bounds the yield surface in hydrostatic compression, provides an inelastic hardening mechanism to represent plastic compaction, and helps to control volume dilatancy when the material yields in shear by providing softening as a function of the inelastic volume increase created as the material yields on the Drucker-Prager shear failure and transition yield surfaces. The cap

surface hardens or softens as a function of the volumetric plastic strain: volumetric plastic compaction (when yielding on the cap) causes hardening, while volumetric plastic dilation (when yielding on the shear failure surface) causes softening. The cap yield surface is written as:

$$F_c = \sqrt{(p - p_a)^2 + \left[\frac{Rq}{1+\alpha-\frac{\alpha}{\cos\beta}}\right]^2} - R(d + p_a.\tan(\beta) = 0 \tag{2.5}$$

where R is a material parameter (between 0.0001 and 1000.0) that controls the shape of the cap, α is a small number (typically 0.01–0.05) used to define a smooth transition surface between the shear failure surface and the cap, and p_a is an evolution parameter that represents the volumetric plastic strain driven hardening/softening. The hardening/softening law is a user-defined piecewise linear function relating the hydrostatic compression yield stress, p_b, and the corresponding volumetric inelastic (plastic and/or creep) strain. Here, only volumetric plastic strain ε_v^p is considered, we have:

$$p_b = f(\varepsilon_v^p) \tag{2.6}$$

The volumetric plastic strain can be expressed as:

$$\varepsilon_v^p = \ln\left(\frac{\rho}{\rho_0}\right) \tag{2.7}$$

Where ρ is the current relative density, and ρ_0 is the initial relative density on filling of die. The evolution parameter ρ_a is given as:

$$p_a = \frac{p_b - R_d}{(1+R.\tan\beta)} \tag{2.8}$$

The transition surface is defined as:

$$F_t = \sqrt{[p - p_a]^2 + \left[q - \left(1 - \frac{\alpha}{\cos\beta}\right)(d + p_a.\tan\beta)\right]^2} - \alpha(d + p_a\tan\beta) = 0 \tag{2.9}$$

To determine the plastic flow rule, the plastic potential is defined by an associated component (that is, a potential function G_c that is equivalent to the cap yield surface F_c) on the cap and a non-associated component on the failure and transition regions. The associated flow potential component in the cap region is defined as:

$$G_c = \sqrt{(p - p_a)^2 + \left[\frac{Rq}{1+\alpha-\frac{\alpha}{\cos\beta}}\right]^2} \tag{2.10}$$

The non-associated flow component in the failure and transition regions is defined as:

$$G_s = \sqrt{[(p_a - p).\tan\beta]^2 + \left[\frac{q}{1+\alpha-\frac{\alpha}{\cos\beta}}\right]^2} \tag{2.11}$$

The two elliptical portions, G_c and G_s, form a continuous and smooth potential surface.
To uniquely define each of the yield surfaces, six parameters are required: β, d, p_a, R, p_b and α, for which β, d, R and p_a are functions of the relative density. The friction angle β and cohesion d are needed to define the Drucker-Prager shear failure surface; the cap eccentricity parameter R and evolution p_a are required to define the cap surface, and p_b as a function of the volumetric plastic strain is required to define the cap hardening/softening law; α is required to define the transition surface.

2.2. Metal modelling

There are two common types of metal plasticity laws available in commercial finite element codes, isotropic or kinematic hardening.
Both plasticity laws are defined in the von Mises stress space and are applicable to ductile metals such as steel (Chen and Han, 1988). Isotropic hardening is typically implemented for a single loading condition, i.e. compressing a column to failure, while kinematic hardening is useful for simulating cyclic loadings or combining different loading states, e.g., cold bending followed by loading to collapse. In this paper because of the cyclic loading implemented to the system, kinematic hardening plasticity law is used to model the reinforcement steel behaviour.

2.2.1 Isotropic hardening

Isotropic hardening is represented with an expansion of the von Mises ellipsoid as the effective stress, σ_e , exceeds the yield stress, σ_{yield} (Fig. 2.2), where:

$$\sigma_e = \frac{1}{\sqrt{2}}\sqrt{(\sigma_1 - \sigma_2)^2 + (\sigma_2 - \sigma_3)^2 + (\sigma_3 - \sigma_1)^2} \tag{2.12}$$

It follows OAB and then springs back along BR as shown in Fig. 2.2a and Fig. 2.2b the slope of the lines in Fig. 2.2b is equal to Poisson's ratio, ν, which is assumed equal to 0.30 for elastic deformation and 0.50 for plastic deformation. The presence of residual stresses after cold bending is denoted with the offset of point R from the origin.

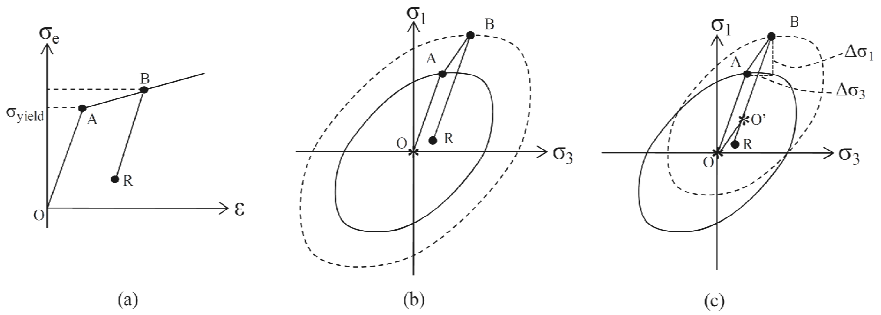

Figure 2.2. Hardening with residual stresses from cold bending: (a) stress-strain curve, (b) isotropic hardening with expanding yield surface, and (c) kinematic hardening with shifting yield surface (Gao and Moen, 2010)

2.2.2. Kinematic hardening

Kinematic hardening is defined with the same Von Mises ellipsoid employed for isotropic hardening. However as the stresses exceed σ_{yield} along AB in Fig. 2.2c, the center of the yield surface permanently shifts to accommodate the imposed stress. The shifting yield surface is a fundamentally different type of yielding behaviour than isotropic hardening (Fig. 2.2b). The new location of the yield surface is defined by the backstress components $\Delta\sigma_1$ and $\Delta\sigma_3$.
After the yield surface has shifted, unloading occurs elastically along B to R, terminating at a nonzero residual stress. If the steel is now loaded again in the same direction as the original loading (again along the line OA in Fig. 2.2c), the apparent yield stress is increased. However, if the steel is loaded in the opposite direction along OA (i.e. −σ1 and −σ3), the yield surface (dashed ellipsoid) is reached with a lower apparent yield stress. This asymmetric yield behaviour has been documented in experiments and is commonly referred to as the Bauschinger effect (Chajes et al., 1963). It is hypothesized that the cyclic nature of the loadings applied to cold-bend members, initiating with plastic bending, followed by elastic springback, and then applied load in service, requires a combination of isotropic and kinematic hardening to accurately simulate structural behaviour. A finite element parameter study follows which explores how the choice of plasticity law and the inclusion or exclusion of residual stresses and effective plastic strains from cold-bending influences load-deformation response (Gao and Moen, 2010).

2.3. Concrete modelling
2.3.1 Concrete in compression

The origin of the concrete model goes back to (Drawin and Pecknold, 1974). In modern terminology, it describes a nonlinear elastic–plastic damage model with a softening range. Since it is based on one- and two-dimensional experiments, originally on those of (Karsan and Jirsa, 1969; Kupfer et al., 1969), its character is rather empirical. It is exactly this property that makes it attractive for theoretical, normative and experimental additions.
The model is orthotropic in the principal stress directions of the biaxial state. Its advantage clearly lies in its compact formulation through introduction of equivalent uniaxial strains. This leads to a description for monotonic as well as for cyclic processes using only four material parameters and a series of rules. In the present work, several aspects of the model are modified with respect to (MC 90 CEB-FIP, 1990) the latter probably being today's most widely accepted basis for reinforced concrete analyses.

2.3.2. Monotonic loading

The stress–strain relationship is defined in the principal stress directions (i) using equivalent uniaxial strains. Here a constitutive law originally published by (Saenz, 1964) will be used:

$$\sigma_i = \frac{\varepsilon_{iu} E_0}{1+\left[\frac{E_0}{E_s}-2\right]\frac{\varepsilon_{iu}}{\varepsilon_{ic}}+\left[\frac{\varepsilon_{iu}}{\varepsilon_{ic}}\right]^2}\ ,\ \varepsilon_{ic} \le \varepsilon_{iu} \le\ 0 \tag{2.13}$$

But the model in (MC 90 CEB-FIP, 1990) may also be employed without loss of accuracy. In Eqn. 2.13, ε_{ic} denotes the equivalent uniaxial strain at the biaxial strength σ_{ic}, the latter depending on the uniaxial compression strength f_c and the ratio of the principal stresses $\alpha = \frac{\sigma_1}{\sigma_2}$ $(\sigma_1 \ge \sigma_2)$. E_0 is Young's modulus at $\varepsilon_{iu} = 0$ and E_S stands for the secant modulus at ε_{ic}. The strain softening branch starts as a straight line at σ_{ic} and ends with $0.2\sigma_{ic}$ at $\varepsilon_{iu} = (1+n)\varepsilon_{ic}$:

$$\{\varepsilon_{iu}\ , \sigma_{ic}\} \Rightarrow \{(1+n)\varepsilon_{ic}\ , 0.2\sigma_{ic}\} \tag{2.14}$$

According to (Drawin and Pecknold, 1974) the number n has been chosen to 3.0, and the condition has been assumed:

$$\frac{E_0}{E_s} \ge 2 \tag{2.15}$$

Most important from the modern understanding of strain softening processes (Bazant and Cedolin, 1980) or (MC 90 CEB-FIP, 1990) is the fact that the constitutive description Eqn. 2.13 and Eqn. 2.14 in the fracture limit holds only for diffuse fracture processes, in which the crushing energy G_c as scale-independent material parameter of concrete is predominantly formed by contributions G_{cu} from (uniformly) distributed microcracking processes. Whenever strain localization as source of compression failure appears (Vonk, 1992), or must be captured by a particular analysis, the then predominant part G_{cl} of the total localized crushing energy renders the description Eqn. 2.13 and Eqn. 2.14 scale-dependent. To counteract this ill-posedness, the factor n in Eqn. 2.14 has to be modified such that the volume-specific crushing energy content, the integral below the stress–strain curve in Fig. 2.3, equals

$$g_{cl} = \frac{G_{cl}}{l_{eq}} \quad \text{for } (1+n)\varepsilon_{ic} \le \varepsilon_{iu} \le \varepsilon_{ic} \tag{2.16}$$

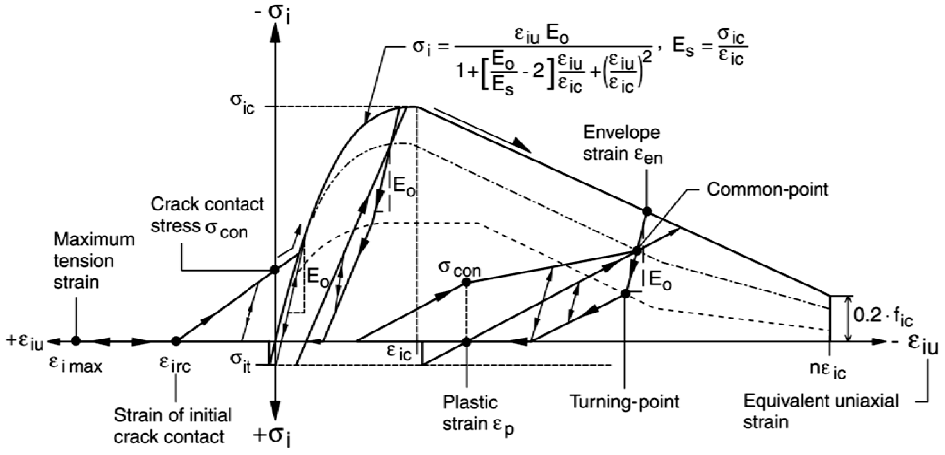

Figure 2.4. Constitutive law of concrete in principal stress system (Noh et al., 2003)

Herein, l_{eq} denotes a suitable internal length scale, e.g. the dimension of the applied finite elements perpendicular to the localization zone (Polling and Kratzig). Often this modification Eqn. 2.16 is suppressed, then the description Eqn. 2.13 and Eqn. 2.14 will be unable to correctly describe compression failure with localization. In spite of such deficiencies, the model may yield good results for all problems in which localization phenomena in compression failure are not dominant.

2.3.3. Cyclic actions

The basic assumption for load cycles stipulates that the monotonic stress–strain curve Eqn. 2.13 and Eqn. 2.14 forms an envelope for all cyclic actions. To them, all plastic and damaging mechanisms including energy dissipation are related. If a particular point $(\varepsilon_{en}, \sigma_{en})$ on the monotonic response curve has been reached, where the strain reverses, the backwards path starts, as in classic plasticity, with negative slope-E_0 until the turning point $(\varepsilon_{tp}, \sigma_{tp})$ has been reached. The locus of the turning points in the complete compression domain is determined by:

$$\sigma_{tp} = \frac{1}{2}\sigma_{en} \quad \text{if} \quad \varepsilon_{en} \geq \varepsilon_{ic} \ \text{ or } \sigma_{en} \leq f_c \tag{2.17}$$

$$\sigma_{tp} = \frac{1}{2}f_c \quad \text{and} \quad \sigma_{tp} \geq 2\sigma_{cp} - \sigma_{en} \quad \text{else.} \tag{2.18}$$

In the turning point $(\varepsilon_{tp}, \sigma_{tp})$ the damage mechanism is switched on, such that from now on the unloading path flattens, containing plastic and damage contributions.
This path is directed towards the point $(\varepsilon_{ip}, \sigma_i = 0)$ where the plastic strain ε_{ip} can be evaluated for the starting envelope strain ε_{en} from the relation:

$$\frac{\varepsilon_p}{\varepsilon_{cu}} = 0.145\left(\frac{\varepsilon_{en}}{\varepsilon_{cu}}\right)^2 + 0.13\left(\frac{\varepsilon_{en}}{\varepsilon_{cu}}\right) \tag{2.19}$$

Herein, ε_{cu} stands for the critical uniaxial strain corresponding to the one-dimensional compression strength f_c. Additionally, from the point $(\varepsilon_{ip}, \sigma_i = 0)$ the reloading path is directed towards the common point $(\varepsilon_{cp}, \sigma_{cp})$, the locus of which can be found from:

$$\sigma_{cp} = \min\left(\frac{5}{6}\sigma_{en}, \sigma_{en} - \frac{1}{6}f_c\right) \leq \frac{1}{3}\sigma_{en} \tag{2.20}$$

A brief review of the model follows: Obviously, because of Eqn. 2.13, plastic and damaging actions start immediately at the origin$(\varepsilon_{iu}, \sigma_i = 0)$, which is not in accordance with modern concepts, where until $0.4\,\sigma_{ic}$ concrete generally is considered as linear elastic. Exchanging Eqn. 2.13 by the stress–strain curve from (MC 90 CEB-FIP, 1990) cures this deficiency. As we observe from Fig. 2.3, the locus of the common points determines the reloading direction, which becomes flatter (with growing

damage) for increasing strain. The locus of the turning points controls the energy dissipation such that the lower σ_{tp} lies, the larger the dissipation becomes (Noh et al., 2003).

3. MODELING

The finite element analysis is carried out by 3D solid elements with 4 or 3 integration points for wall and soil elements. Truss element is used for rebars which is embedded in the concrete elements.

The finite element mesh of the retaining wall is shown in Fig. 3.1 It is assumed that that the length of filling soil affecting the behaviour of retaining wall is fivefold of the wall height (5H), the wall is supported rigidly from the base and vertical boundaries are held in horizontal direction (Gursoy and Durmus, 2009). In this study, small elements are used especially for the retaining wall and the soil models close to it on which stress and strain are very important.

Some models generated to consider the effect of friction angle of the soil in the maximum deflection of the wall's top point during the ground acceleration of El Centro earthquake record. Then the time history analysis of quay walls with and without counterfort is investigated by the ground acceleration of El Centro earthquake record Fig. 3.2 the ground acceleration records are scaled to PGA of maximum 0.5g. Rayleigh damping coefficients (Bathe, 1982) are calculated for these models.

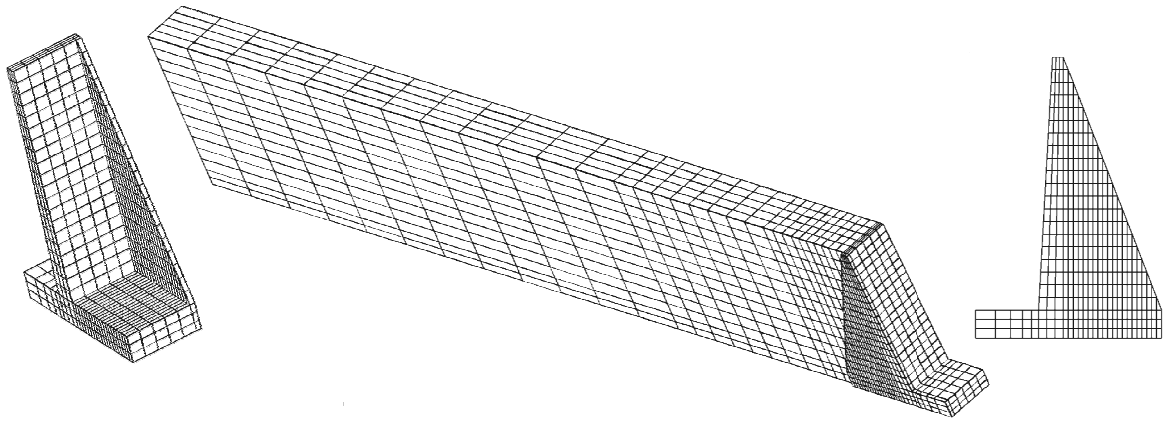

Figure 3.1. Finite element mesh of the retaining wall.

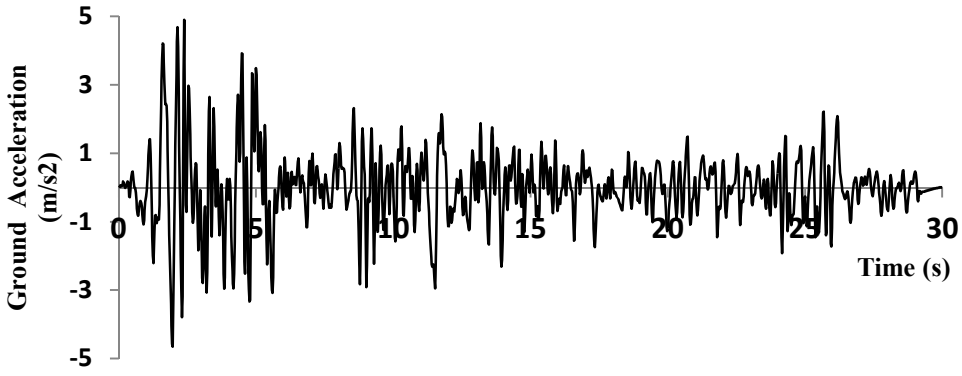

Figure 3.2. Ground acceleration of El Centro earthquake

The soil-structure interaction was considered in the model by means of two surfaces. A frictional contact/separation algorithm has been used at the structure interfaces with the soil to take into consideration the nonlinearity state of the soil-wall interactions. These two surfaces can transmit contact pressure and frictional shear stress. The surfaces can separate from each other and could not penetrate to other.

4. RESULTS

4.1. Time history of the principle stress σ_z in the bottom of wall:

The time history of the normal stress σ_z is shown in Fig. 4.1 during the earthquake. It is clear that the maximum of the σ_z happens nearly to the maximum PGA of the earthquake record.

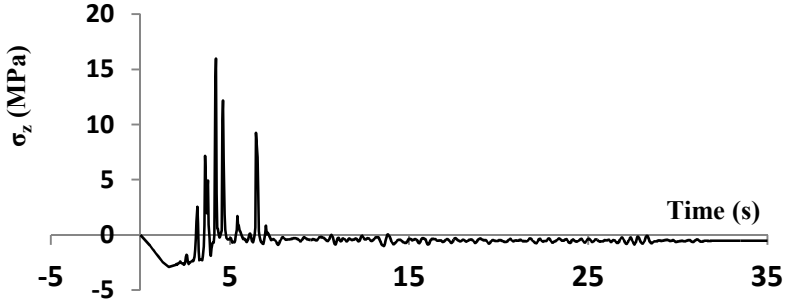

Figure 4.1. Principle stress σ_z in the bottom of wall

The relative displacement between top and bottom of the wall during the earthquake is shown in Fig. 4.2.

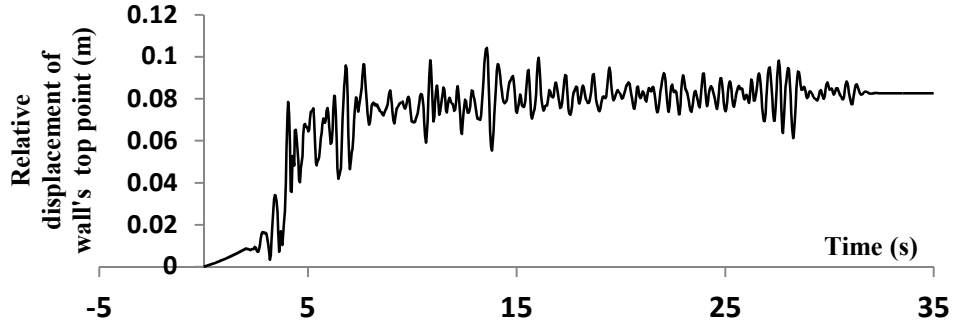

Figure 4.2. Relative displacement of wall's top point

4.2. Effect of friction angle on active soil pressure during the earthquake

Two models are generated with the same geometric parameter and material behaviour, the only deferent is the amount of friction angle of the soil. The response of these two structures is demonstrated in Fig. 4.3. It can be seen that by increase in the amount of friction of the soil the top wall point displacement decrease during the earthquake.

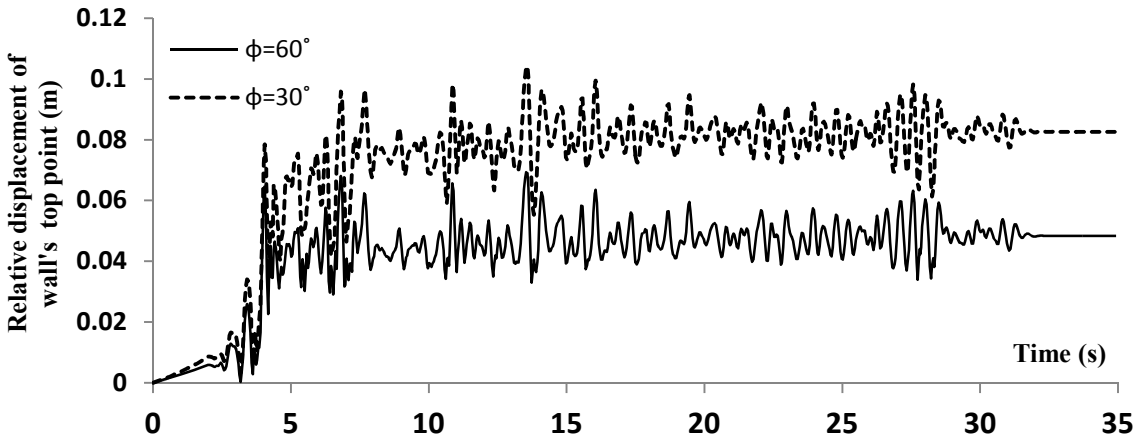

Figure 4.3. Seismic behaviour of wall with different amount of friction angle.

4.3. Effect of counterfort on seismic response of the wall's top point

The comparison of using counterfort is demonstrated in the Fig. 4.4. Two models with the same volume of concrete material are made to compare the seismic behaviour of the quay walls with or without counterfort. The geometry specification of these two blocks is shown in Table 4.1. and the material parameters are the same with Table 4.2.

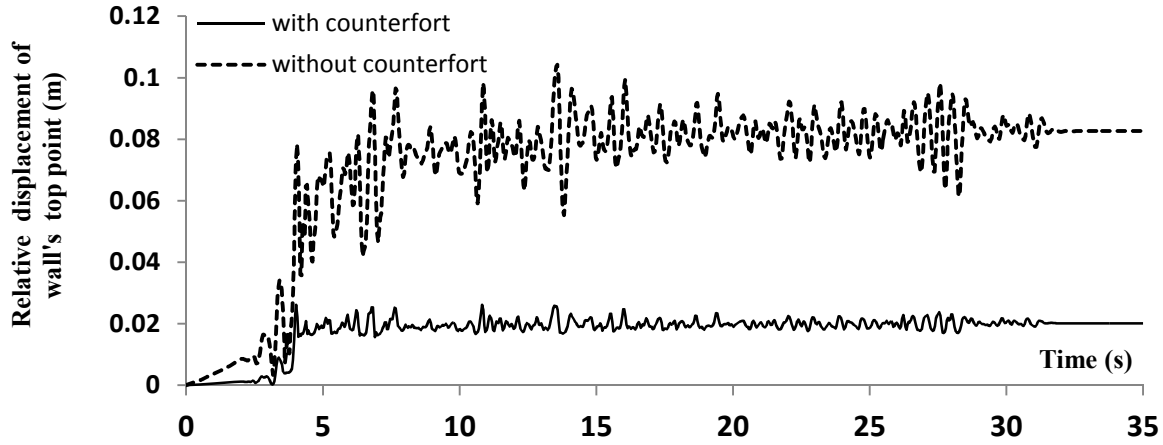

Figure 4.4. Seismic behaviour of wall with or without counterfort

Table 4.1. Wall property of the model

Wall property	Without counterfort	With counterfort
	Value (m)	
Wall-base width	5.3	5.3
Wall-toe width	1.8	2.05
Wall-top thickness	0.3	0.3
Wall-bottom thickness	0.7	0.45
Wall-heel thickness	0.8	0.8
Wall-height	8	8
Counterfort thickness	-	0.3
L-Shaped block length	4.3	4.3
Total concrete volume	33.02 (m^3)	32.61 (m^3)

Table 4.2. soil property of the models

Soil Property	Units	Value
Elastic modulus	MPa	20
Poisson's ratio	-	0.4
Friction angle	degree	30 or 60
Cohiession	KPa	0
Total unit weight	KN/m3	18
Coefficient of the earth pressure at rest	K_0	0.5

5. CONCLUSION

The seismic behaviour of L-shaped retaining wall is investigated by 3D modeling of the wall and the soil behind it considering nonlinear behaviour of soil, concrete and reinforcement materials in addition to soil- structure interaction effect. By increasing the amount of friction angle of the soil, the relative displacement of the wall and the soil deformations during the earthquake are decreased. Moreover, it can be concluded that the usage of counterfort in this type of structures will reduce the structural seismic response, help the system to behave more effectively and make the design more economic.

6. REFERENCE

ABAQUS, (2006). ABAQUS 6.6 Theory Manual. ABAQUS Inc.

Bathe K.J. (1982). Finite Elements Procedures in Engineering Analysis. *Prentice-Hall englewood Cliffs*, NJ.

Bazant ZP, Cedolin L. (1980). Fracture mechanics of reinforced concrete. *ASCE J Eng Mech*;106:1287–306.

Chajes A., Britvec S. J. and Winter G. (1963). Effects of cold-straining on structural steel sheets. *Journal of the Structural Division, ASCE.* **89**(ST2), 1-32,.

Chen, W.F. and Mizuno E., (1990). Nonlinear Analysis in Soil Mechanics: Theory and Implementation. *Elsevier Science Publishing Company Inc.*, New York.

Chen W. F. and Han D. J. (1988), Plasticity for Structural Engineers. Springer-Verlag, New York, NY,.

Drucker D. C., Gibson R. E. and Henkel D. J., (1957). Soil mechanics and work-hardening theories of plasticity. Transactions. *American Society of Civil Engineers.* **122**, 338–346.

Drawin D. and Pecknold DA. (1974). Inelastic model for cyclic biaxial loading of reinforced concrete. Civil Engineering Studies, Report No. SSR 409, University of Illionois, Urbana.

Feenstra PH. (1993). Computational aspects of biaxial stress in plain and reinforced concrete. PhD thesis, Delft Technical University.

Gao T., Moen. D (2010). The cold work of forming effect in steel structural members. *SDSS' Rio 2010 Stability and ductility of steel structures*, Rio de Janeiro, Brazil

Goh A. T. C (1993). Behaviour of cantilever retaining walls. *Journal of Geotechnical Engineering.* **119(11)**,1751-1770.

Gursoy S., Durmus A. (2009). Investigation of linear and nonlinear of behaviours of reinforced concrete cantilever retaining walls according to the earthquake loads considering soil-structure interaction. *Structural Engineering and Mechanics.* **31(1)**,75-91.

Jurukovski, D. and Rakicevic, Z**.** (2004). Structural Retrofitting of A 6-Storey Hotel with HDRB and Viscous Dampers. *Third European Conference on Structural Control.* **Vol. II:** S6-92-S6-95.

Karsan ID, Jirsa JO. (1969). Behaviour of concrete under compressive loadings. *ASCE J Struct.* Div, **(95)**, 2543–2563.

Kim S. R., Kwon O. S., Kim M. M. (2004). Evaluation of force components acting on graviity type quay walls during earthquakes. *Soil Dynamics and Earthquake Engineering.* **24**, 853-866.

Kolathayar S., Ghosh P. (2009). Seismic active earth pressure on walls with bilinear backface useing pseudo-dynamic approach. *Computers and Geotechnics.* **36**, 1229-1236.

Kupfer HB., Hilsdorf HK, R€usch H.(1969). Behaviour of concrete under biaxial stresses. ACI **J;66,** 656–666.

Kuwano J., Takahashi A., Hiro-oka A. and Yamauchi K. (1999). Shaking table tests on caisson type quay-wall in centrifuge. *2nd International Conference on Earthquake Geotechnical Engineering, Lisboa, Portugal.* **Vol. 1**, 365-370.

Kwak H.G., Kim S-P. (2002). Nonlinear analysis of RC beams based on moment-curvature relation. *Computer and Structures*; **80**(6), 15–28.

Kwak H.G., Fillipou FC. (1990). Finite element analysis of reinforced concrete structures under monotonic loads. Report UCB/SEMM-90/14, University of California, Berkeley.

Madabhushi S. P. G. and Zeng X. (1998). Seismic response of gravity quay walls. II: Numerical modeling. *J. Geotech. Geoenviron. Eng.,* **124(5)**, 418-427.

MC 90 CEB-FIP Model Code (1990), Design Code Lausanne: Comit-e Euro-International du B-eton, Bulletin d_Information 195.

Noh S. Y., Kratzig W. B., Meskouris K. (2003). Numerical simulation of serviceability, damage evolution and failure of reinforced concrete shells. *Computers and Structures* **81**, 843-857.

Polling R., Kratzig WB. An elasto-plastic damage theory for reinforced concrete with minimum number of material parameters. *Comput Struct*, submitted for publication.

Saenz IP.(1964). Discussion to Equation for the stress–strain curve of concrete by Desayi and Krishnan. *ACI J*;**61**: 1229–1235.

Sandler, I.S., (2002). Review of the development of cap models for geomaterials. In: *15th ASCE Engineering Mechanics Conference*, Columbia University, New York.

Scott BD, ParkR, Priestley MJN. (1982). Stress–strain behaviour of concrete by overlapping hoops at low and high strain rates. *ACI J*;**79:**13–27.

Shanley F. R. (1957), Strength of Materials. McGraw-Hill Book Company, New York, NY.

Vonk RA. (1992). Softening of concrete loaded in compression. PhD thesis, Delft Technical University.